

DOT tomography of the solar atmosphere

IV. Analysis of a surge from champion region AR10486

K. Tziotziou¹, G. Tsiropoula², and A.G. de Wijn¹

¹ Sterrekundig Instituut, Utrecht University, Postbus 80 000, 3508 TA Utrecht, The Netherlands
e-mail: K.Tziotziou@astro.uu.nl; A.G.deWijn@astro.uu.nl

² National Observatory of Athens, Institute for Space Applications and Remote Sensing, Lofos Koufos, 15236 Palea Penteli, Greece
e-mail: georgia@space.noa.gr

Received / Accepted

Abstract. We present Ca II H high temporal and spatial resolution observations of active region AR10486 when found near the solar limb obtained by the Dutch Open Telescope (DOT). This active region was also observed by the Transition Region and Coronal Explorer (TRACE) and is the same region which some hours later produced the largest X-flare ever recorded. We focus our study on a surge observed by DOT with a remarkable clarity and by TRACE. In TRACE images the surge could be followed for at least 2.5 hours at almost the same place shrinking and expanding several times. From DOT images we found outward propagating intensity disturbances. Applying a wavelet analysis we also found brightness oscillations with ~ 6 min and 3 min periodicities...

1. Introduction

The solar chromosphere is the region where the switch from the dense, matter-dominated photosphere to the tenuous corona is taking place. Just as it is now clear that this region is of major importance in understanding processes in the outer atmosphere, such as the solar wind and coronal heating, it seems equally clear that it is the least understood region of the solar atmosphere.

The solar chromosphere is a highly inhomogeneous region, full of structures of different intensities, shapes and sizes. In active regions gas ejections are very usually observed which manifest themselves as moving prominences on the limb. One type of such ejections is a “surge”, which typically has the form of a straight or slightly curved spike. $H\alpha$ surges have been studied for over 50 years (see Roy 1973a, 1973b). They reach heights of up to 200 Mm, with peak velocities of 50-200 km s⁻¹ and then fade or fall back to the chromosphere, apparently along the trajectory of ascent (Svestka 1976; Tandberg-Hanssen 1977; Schmieder et al. 1994). They typically last 10-20 min. They are evolving over a small dark mound-like region forming an inverted “Y” configuration. It is suggested by Kurokawa & Kawai (1993) that this shape could be explained by a magnetic reconnection model. Observations show that surges are usually associated with small, changing satellite sunspots which represent islands of polarity reversal (Rust 1968; Canfield et al.

1996) situated close to the edges of sunspot penumbrae or with newly magnetic flux emergence in close proximity to an opposite polarity pre-existing flux (Yoshimura et al. 2003) and provide additional evidence in support of a reconnection model. Such models have already been proposed (Canfield et al. 1996; Yokohama & Shibata 1996).

Apart from surges several other structures are observed at the quiet and active chromosphere. The network boundaries, which seemingly border the photospheric supergranule cells, are the locus of most of the quiet chromosphere fine structures, known as mottles when seen on the disk. Their most likely limb counterparts are spicules. In active regions one can see bright and dark elongated structures similar to the dark and bright mottles, although, usually, more extended. These are referred to as fibrils. Fibrils are also called the bright and dark structures that give the filamentary appearance of sunspots penumbrae and superpenumbrae. According to Foukal (1971) mottles and fibrils are similar structures, the latter being more inclined than the former relative to the line-of-sight (LOS) due to the different inclinations of the local magnetic field.

In Tziotziou et al. (2004) we applied a wavelet analysis and found that intensity and velocity variations in dark mottles in a quiet region have a dominant period of ~ 5 -6 min. The same behaviour we found for fibrils in the periphery of a plage. 5-6 min oscillations in dark fibrils have also been reported by De Pontieu et al. (2003), who, furthermore, suggested p-modes as their driver. To our knowledge no observations of any kind of periodicities in surges have been reported so far.

Send offprint requests to: K. Tziotziou,
e-mail: K.Tziotziou@astro.uu.nl

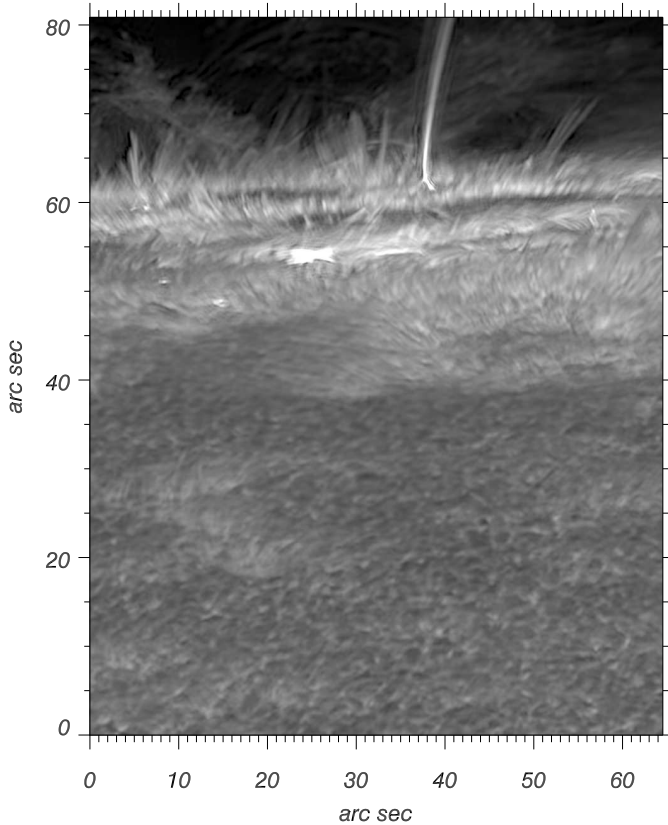


Fig. 1. A sample DOT Ca II H filtergram illustrating the intricate structure of the chromosphere. The dark structures near the limb are sunspots, while the bright large-scale cellular pattern at the bottom of the image is the chromospheric network. Sunspots, a surge and numerous jet-like structures are clearly visible on the limb.

Apart from the differences in scales (length, time and velocity) there is a strong similarity between a mottle (or spicule) and a surge. Both structures have a strong recurrence tendency and often repeat themselves at apparently the same place several times. Moreover, they carry the signature of the underlying magnetic field and are thought to be associated with magnetic reconnection. It is thus possible that they are the manifestation of the same phenomenon occurring on different scales. In this context, detailed study of the dynamical evolution of individual structures is important in understanding the characteristics of the magnetic field and the nature of the physical processes which produce them.

In the following sections we report high spatial and temporal resolution Ca II H observations of the solar limb obtained by the Dutch Open Telescope (DOT). Active region AR10486 which some hours later produced the largest X-flare ever recorded is included in these observations. We then focus our study on a surge which is observed with a remarkable clarity in DOT images and also in UV and EUV images obtained by the Transition Region and Coronal Explorer (TRACE).

2. Instruments and data reduction

The observations used in this study, were obtained on November 4, 2003 by DOT (Rutten et al. 2004). DOT recorded

image sequences between 16:21:20 and 16:47:35 UT in its Ca II H passband. The filter was tuned to the line core at 3968 Å and has a bandwidth of 1.35 Å. Speckle bursts of 100 frames each were taken at a rate of 6 frames s⁻¹ by a fast CCD camera. The individual frames were speckle reconstructed (see Rutten et al. 2004 for details) and carefully aligned yielding one reconstructed image per burst. The final time sequence consists of 63 frames of 1140 pixels × 910 pixels with an angular resolution of 0.071''/pixel and at 25 s cadence. TRACE (Handy et al. 1999) was also observing the same region on November 4, 2003 between 14:30:12 and 18:29:43 UT in the 1600 Å and 195 Å passbands. The respective cadences are 39 ± 9 s and 43 ± 13 s, but there are some gaps of several minutes in the observations, (however not during the DOT time sequence. TRACE images have a field of view of 768 pixels × 768 pixels and are at full resolution (1 pixel = 0.5''). All data have been corrected for a constant dark current, a CCD readout pedestal value of 87 Data Numbers (DN), hot pixels and radiation spikes due to cosmic rays, and have been co-aligned by a cross-correlation technique to correct for solar rotation and spacecraft pointing jitter. For the co-alignment subsequences of 20 frames were aligned to the last previously aligned frame. A 5 × 5 pixel boxcar smoothed running average over nine of these coarsely aligned frames was produced, and finally each frame was aligned to this running average. TRACE images were used for comparison with DOT's images. TRACE-DOT co-alignment was done by choosing corresponding images observed almost at the same time (~16:40 UT) and using standard IDL solar software based on recognition of solar features.

3. Description of the observations

The present DOT Ca II H observations must be included among the best high-resolution observations of the solar limb ever recorded. In Fig. 1 a sample of these observations is presented. At the lower part of the image the quiet Sun with the chromospheric network as a bright large-scale cellular pattern is clearly seen. Several individual, round or elongated, mainly bright but also dark structures are found all over the quiet solar region, usually fanning out from the network in a bushlike arrangement. Their evolution is very complex, since they undergo substantial changes in brightness and length with time. There are several examples of structures which after fading they reappear at almost the same position. An active region is clearly visible at the top of Fig. 1. This is active region AR10486, which produced the largest X-flare ever recorded starting around 19:36 UT, almost three hours later from the beginning of DOT's observations. The large, dark structures near the limb are the umbrae of sunspots. Around their periphery a fairly regular penumbral structure is seen consisting of numerous bright fibrils, packed close together and observed with a remarkable clarity. The inner ends of the fibrils are more or less at right angles to the borders of the adjacent parts of the umbrae, although there are some of them that are clearly bent forming small loops (see Fig. 1 at the region included between ~ 50''- 60'' in the X direction and ~ 57''- 60'' in the Y direction). Fibrils are very similar to spicules in appearance and it is impossible to distinguish whether structures seen exactly

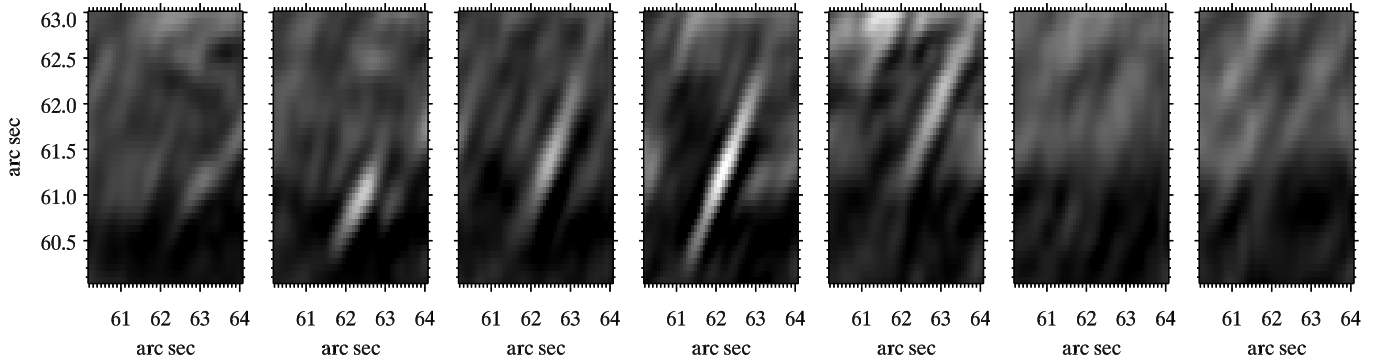


Fig. 2. Temporal evolution of a fibril observed with DOT. The coordinates in the x and y axes correspond to the same coordinates of Fig. 1. The presented sequence starts at 16:22:35 UT and the time cadence is 75 s.

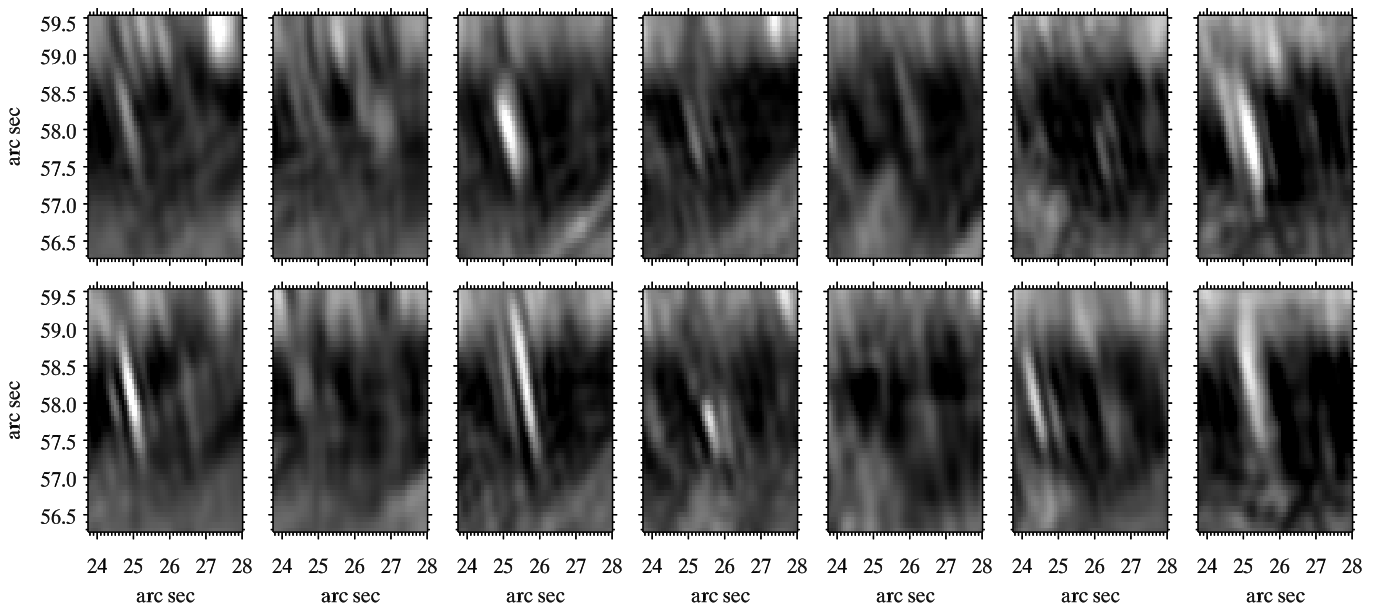


Fig. 3. Two fibrils observed with DOT showing recurrent behaviour. The coordinates in the x and y axes correspond to the same coordinates of Fig. 1. The presented sequence starts at 16:25:55 UT (top left image) and the time cadence is 75 s (time runs from top to bottom and from left to right).

at the limb are the one structure or the other. Individual fibrils seem to have heights of $\sim 2''$ - $3''$ (probably because only their lower parts are visible) and are very narrow, often appearing to be less than $0.5''$ in width. When they are not overlapped by other structures, it is easy to follow their evolution, which is quite complex. Some of them, despite changes in brightness, size and shape are observed to persist for the whole time sequence. Such an example is shown in Fig. 2: the fibril begins as a circular bright structure and then elongates and attains a maximum length. It then becomes fainter, but it remains visible till the end of the sequence. Other structures reappear several times at the same place (see Fig. 3 for a characteristic example) in periods of a few minutes. The solar limb is protruded by a myriad of bright jets with footpoints located in front or behind the limb. Among them is a remarkable surge. The surge, already in progress when DOT's observations began, appears in emission and it is a standing alone structure. It has the form of a slightly

curved jet and fits the “Eiffel Tower” description of Kurokawa & Kawai (1993): it is evolving over a small dark mound-like region forming an inverted “Y” configuration. In the same work these authors suggested that this shape could be explained by a magnetic reconnection model. It is not possible to make, direct comparison of the present active region with photospheric magnetograms recorded by the Michelson Doppler Imager (MDI) on-board the Solar Heliospheric Observatory (SOHO), since this region is nearly at the limb. However, magnetograms of the previous days show that there are ample, evolving magnetic fields of both polarities in the region from where the surge is ejected. It is thus very likely that the energy required to expel the gas in the surge is produced by reconnection events at its base. The surge extends upward beyond the DOT field of view with a projected extent of more than 14 Mm. Its base is sometimes obscured by fluxtubes, and it remains stable throughout the 26-minute duration of the DOT sequence.

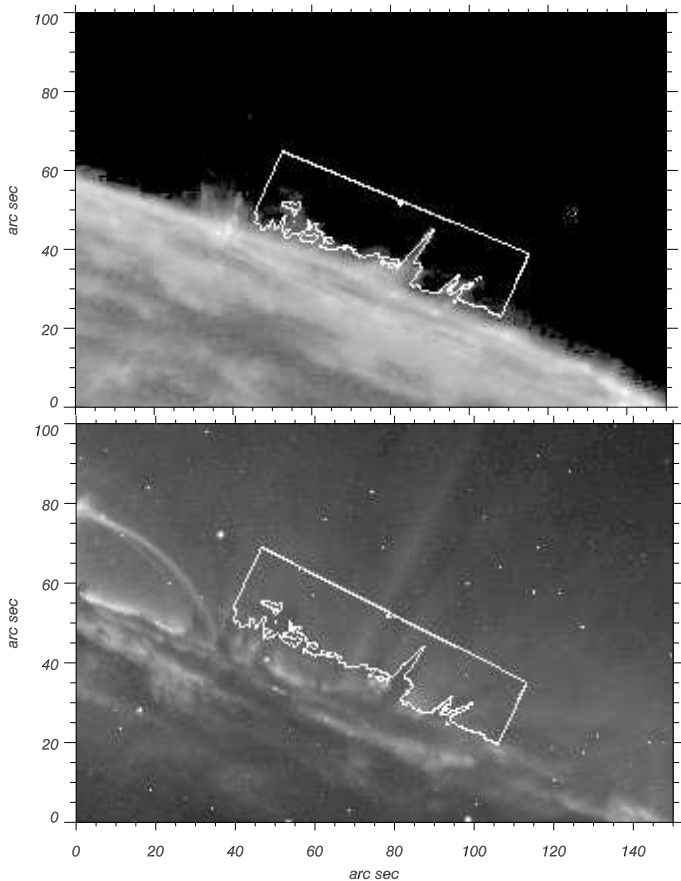


Fig. 4. TRACE 1600 Å image (top) and 195 Å image (bottom) with overlotted white contours of the DOT Ca II H data.

In Fig. 4 contours of a DOT image have been overlotted to the TRACE 1600 Å (top) and 195 Å (bottom) images taken at nearly the same time. The former TRACE image samples plasma at low temperatures ($\sim 10^4$ K), but also includes the C IV emission from plasma of $\sim 10^5$ K. The latter samples plasma at temperatures of $\sim 1.4 \times 10^6$ K. The surge appears in emission in the 1600 Å, as in the Ca II H passband. From this we may conclude that the surge consists of relatively cold, $\sim 10^4 - 10^5$ K, gas. On the other hand comparison of the DOT Ca II H and TRACE 195 Å images reveals that the EUV counterpart to the Ca II H bright surge is a dark absorption feature that intercepts the bright $\sim 10^6$ K background. The absorption mechanism is likely to be similar to the longer wavelength suggestion by Kucera et al. (1998) (see also Rutten 1999). According to this suggestion the bound-free extinction is probably dominated by scattering rather than thermal destruction. Such bound-free scattering is not monochromatic because spontaneous recombination (the most likely process to follow radiative ionization) re-emits the absorbed photons preferentially near the ionization threshold. Each bound-free scattering sequence therefore not only redirects a 195 Å photon, but also shifts it out of the TRACE passband. The observed darkness therefore does not measure temperature even for thick structures.

4. Analysis and results

4.1. TRACE-DOT comparison of the surge

The longer duration and the larger field of view of the TRACE observations, permits us to follow the spatial and temporal evolution of the surge in the 1600 Å passband, where it is clearly visible. Fig. 5 shows images of the appearance, development and decay of the surge at selected times. The surge is initiated by a sudden flarelike brightening near the limb at $\sim 16:06$ UT. It is, thus, very likely that the surge is the manifestation of the magnetic reconnection between new and pre-existing magnetic flux. If the new flux is due to newly emerging flux or to the reorganisation of local small scale magnetic fields cannot be proved or ruled out, since the magnetic topology cannot be examined, because the observed region is found nearly at the limb. The brightening at the base persists during the entire duration of the surge and is probably the non resolved base of the inverted “Y” configuration clearly seen in DOT’s images. After the appearance of the bright patch a spiked jet expanded upwards attaining a maximum height of ~ 43 Mm at $\sim 16:24$ UT (see also Fig. 6). The apparent upward velocity is 90 km s^{-1} , although the rise phase of the surge does not exhibit a fairly steady extension of emission to higher altitudes. The surge remains at the maximum height for ~ 5 min, although there are small variations in it with time. It then begins shrinking attaining a lower height at $\sim 16:31$ UT, where it remains till 16:34 UT. It is not clear if the decay phase can be described as simply the reverse of the rise phase with emission moving to lower altitudes or as a fading in place. Then a new ascending phase begins and the surge attains a maximum height of ~ 25 Mm (lower than before) at $\sim 16:38$ UT. Then it becomes shrinking again (Fig. 5 and Fig. 6 at 16:44:34 UT) attaining a new minimum height at $\sim 16:58$ UT. It remains at that height for at least 20 min (between 17:20 and 17:42 UT there is a gap in the observations). Then at $\sim 17:43$ UT it starts elongating again and reaches the same maximum height as in the second phase of elongation. At $\sim 17:02$ UT it becomes shrinking and at 18:23:08 UT is hardly visible, while at 18:25:40 UT is no more visible. Clearly the visible heights are subject to the brightening and decay of the emission in the 1600 Å passband. From the TRACE 1600 Å observations it is clear that the surge lasts for about two and a half hours and has a strong recurrence tendency extending and shrinking at least 3 times during this observation period at apparently exactly the same place.

The height of the surge in the 1600 Å TRACE images can be defined from the visible top of its intensity emission (see Fig. 5). In DOT data, the top of the surge is outside the field-of-view (FOV) and hence its real height can not be measured. However, an “apparent height” can be defined as the height where the Ca II H brightness inside the surge is equal to a certain value (brightness enhancement which changes with time is always observed at the lower part of the surge, see also Fig. 8). The pre-selected brightness value is such, that the maximum obtained apparent height is always lower or equal to the maximum measurable height of the surge due to the limited FOV of DOT. Fig. 6 displays the measured 1600 Å height and the “apparent” Ca II H height of the surge. The dashed line in Fig. 6

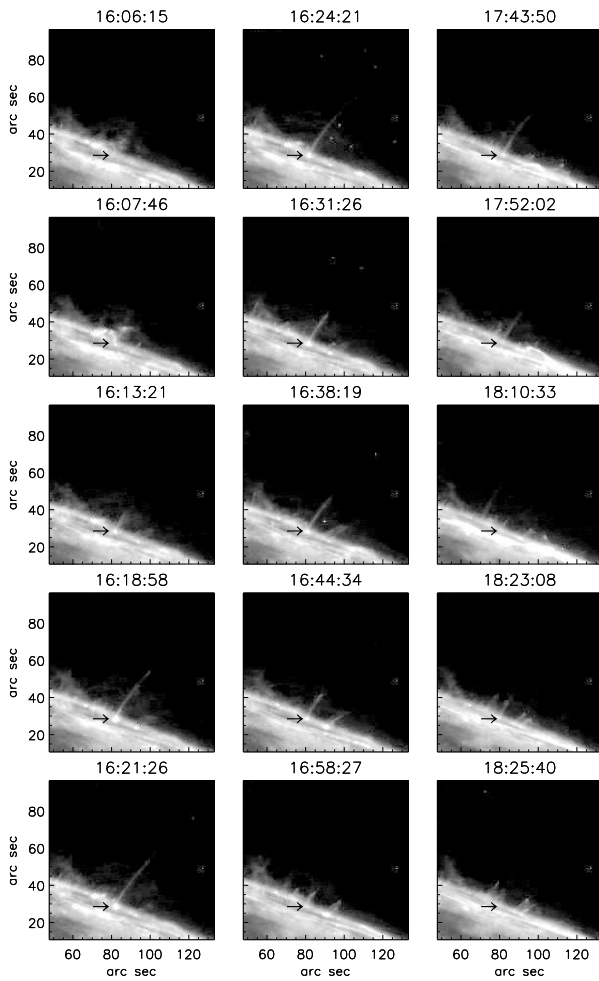


Fig. 5. TRACE 1600 Å images at selected times (time runs from top to bottom). The black arrow points at the base of the surge. Plotted coordinates correspond to those of Fig. 4.

shows the maximum height of the surge that is inside the DOT’s FOV. The origin for the height measurements is indicated by an arrow at Fig. 5 and Fig. 7 and for the latter it coincides with the mound-top of the inverted “Y” configuration. The inclination has been taken into account in both cases for the calculation of the height. The motion of brightness fronts in both temporal sequences might not correspond to true material motion, if the emission fronts were to propagate at a rate different from that of the matter. However, the qualitatively good correspondence between the two curves leads us to believe that both curves represent actual motion of material. It seems also that there is a short time delay between the two curves which is also indicative of an upward material motion.

4.2. Intensity profile of a cut along the surge

In Fig. 7 we present an enlargement of a cut-out of Fig. 1 around the surge area. The position, direction and length of the surge does not change significantly with time in our DOT FOV however its brightness does change. We analyse the brightness

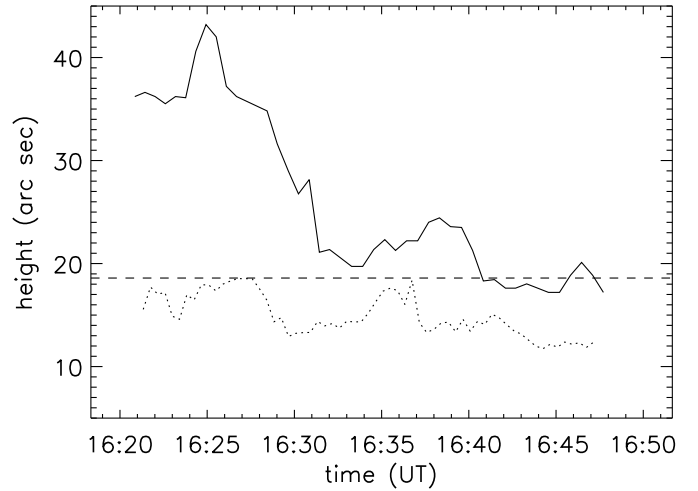


Fig. 6. Maximum height of the surge from TRACE 1600 Å images (solid line) and “apparent” Ca II H height of the surge (see text) from DOT images (dotted line). In both cases the height is measured from the base of the surge and its inclination has been taken into account. The dashed line shows the maximum height of the surge that can be measured in DOT images due to the limited FOV

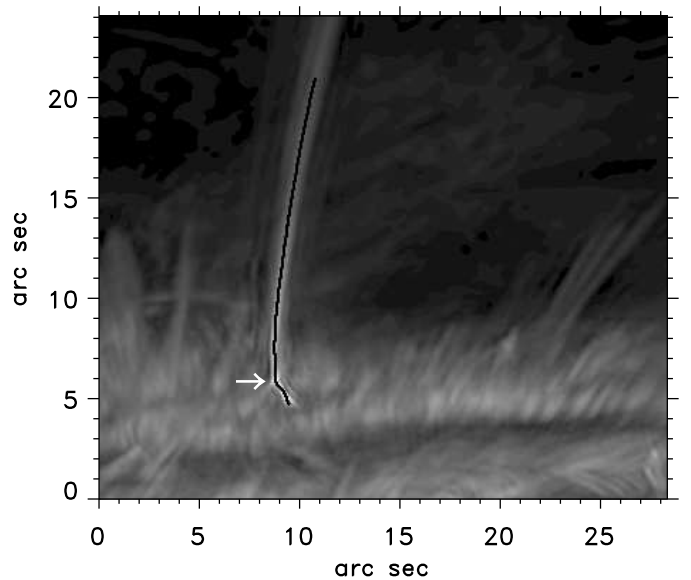


Fig. 7. Enlargement of the DOT observations of the surge area. The black solid line, superimposed on the surge, indicates the cut along the surge used for the time slice image of Fig. 8 and the spectral analysis described in 4.3. The white arrow indicates the mound-top of the inverted “Y” configuration which is also used as the origin for the apparent height calculation of Fig. 6.

variations along the central axis of the surge (time slice image), which is indicated by a black line in Fig. 7. This axis contains the mound-top of the inverted “Y” configuration and its right leg. As we have already mentioned in Sect. 3 this configuration is usually suggested to be associated with magnetic reconnection. We have averaged the intensity over a strip extending 0.14” on either side of the main axis, which is carefully traced on all images of the time sequence as the position of maxi-

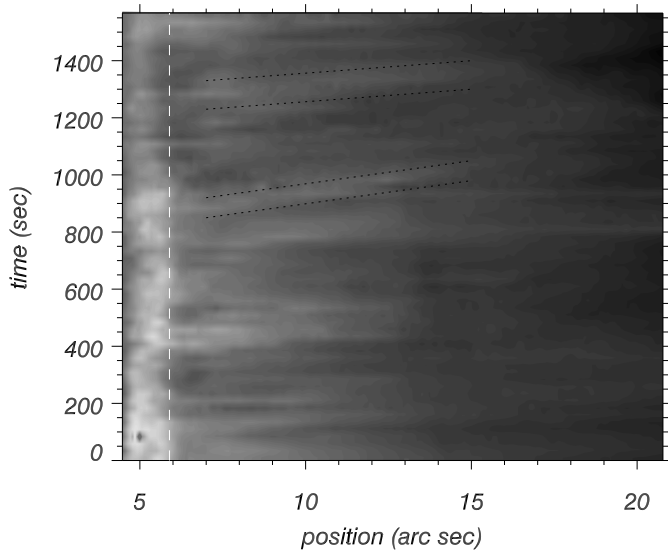


Fig. 8. Brightness along the main axis of the surge (see text and Fig. 7) as a function of position and time. The starting time corresponds to the beginning of the DOT observations at 16:21:20 UT, while position corresponds to the y-coordinates of the cut shown in Fig. 7. The white dashed line indicates the mound-top of the inverted “Y” configuration. The black dotted lines include two bright ridges indicating upward propagating disturbances

imum brightness at each height along the surge. This ensures taking into account small changes in the direction of the surge with time. Fig. 8 shows the brightness along this cut against time. Several bright and dark ridges with respectively higher and lower brightness are visible which indicate the presence of propagating disturbances. The two clearest examples are the brightness enhancements that start at positions (6,1250) and (6,900), presented within black dotted lines in Fig. 8. Positive gradients indicate upward travelling disturbances. By measuring the slope of each ridge we obtain apparent propagation speeds of 75 km s^{-1} and 50 km s^{-1} respectively for these two cases. Since the apparent speed is the component of the speed projected onto the plane of the sky, it represents a lower limit to the propagation speed along the surge. The obtained speeds far exceed the chromospheric sound speed of approximately $10\text{--}20 \text{ km s}^{-1}$ so they have to be associated with upwardly moving material ????. The upper brightness enhancement (origin at 6,1250) stops suddenly at a height of $\sim 10''$. The dark wedge shape starting at that position around 1100 s could be due to impacted downward moving material returning back from above. The same wedge shape is visible for earlier brightness enhancements in Fig. 8. Another possibility is that the wedge shape maybe associated with actual variations of the length and hence brightness of the surge. The possibility that the material becomes optically thin near the top because of expansion cannot be excluded ????.

4.3. Spectral analysis

There is a hint for a periodic variation of the surge apparent Ca II H height in Fig. 6. Furthermore, the time slice image of

Fig. 8 implies some kind of periodicity for the surge brightness. We are using a wavelet analysis to determine the presence and location of oscillations at the base and within the main body of the surge.

Wavelet analysis The wavelet analysis permits the determination of any periodic signal within the series and how this period varies with time. We refer the reader to Torrence & Compo (1998) for a detailed description of the wavelet analysis and to Fludra (2001) for a comparison between wavelet and Fourier analysis results of the same signal. For the wavelet transform we use the Morlet wavelet, which consists of a plane wave modulated by a Gaussian. The cone of influence (hereafter COI), defines the region where effects of zero padding of a finite series become important. Hence periodicities in the COI are doubtful. The global power spectrum is the average of the wavelet power spectrum over time (comprising the whole range of our time series, i.e. inside and outside the COI regions) and is more or less equivalent to the Fourier analysis spectrum. The significance level of any detected period, is determined by comparison of the power spectrum to the background noise spectrum, which in our case is assumed to be Poissonian. A significance level of 95% indicates a 5% probability that any significant power is caused by chance. A randomization test, where the significance of a detected period is calculated with respect to a finite number of random permutations of the observed time series, has been also applied as a more reliable approach. We refer the reader to Banerjee et al. (2001) and Tziotziou et al. (2004) for a detailed description of this method. This method can also be applied for the global spectrum. There is a 3.5% error, due to the finite number of permutations used (equal to 200) for the estimated probabilities. Only power peaks with a period lower than a maximum value, defined as the maximum period of the COI line (hereafter *cut-off period*), are considered for this randomization analysis.

Cross-wavelet spectrum The cross-wavelet transform between two series X and Y with wavelet transforms $W_n^X(s)$ and $W_n^Y(s)$ is defined as $W_n^{XY}(s) = W_n^X(s)W_n^{Y*}(s)$ where $W_n^{Y*}(s)$ is the complex conjugate of $W_n^Y(s)$ (Torrence & Compo 1998). From this complex cross-wavelet transform one can define the *cross-wavelet power* $|W_n^{XY}(s)|$ and the *coherence phase* $\phi_n(s) = \tan^{-1}[\Im\{W_n^{XY}(s)\}/\Re\{W_n^{XY}(s)\}]$, where \Re and \Im are respectively the real and imaginary components of the transform. It can be shown that this phase coherence is analogous to that of the Fourier analysis (Bloomfield et al. 2004). The global phase coherence is the average of the phase coherence over time (comprising the whole range of our time series, i.e. inside and outside the COI regions).

4.3.1. Wavelet analysis within the surge

In Figs. 9 and 10 we present a spectral analysis at positions 5.4 and 8.8'' respectively (see Fig. 8). The former position corresponds to a point within the right leg of the inverted “Y” configuration (see Fig. 7) while the latter at a higher point within the surge well above the mound-top of the inverted “Y” con-

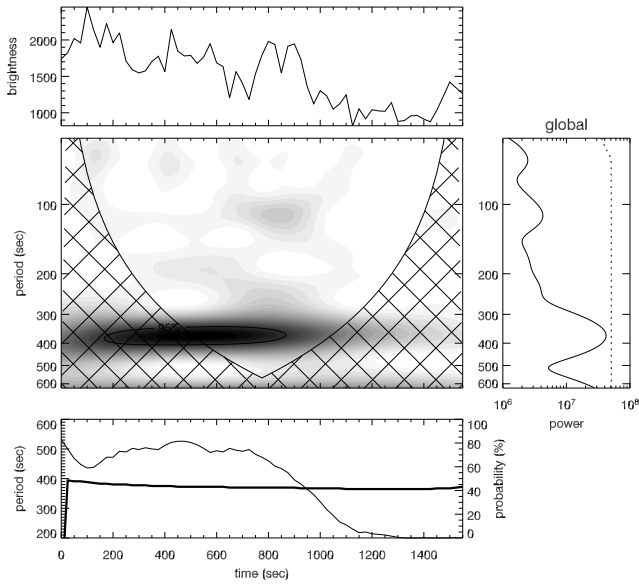


Fig. 9. Wavelet analysis of the brightness (in counts) of the surge at position 5.4'' (see Fig. 8). The middle left panel shows the time-period calculated power spectra for the brightness variations shown in the top panel with black representing high values of power (contours represent the significance level of 95%). Cross-hatched regions indicate the COI regions. The middle right panel shows the global power spectrum, i.e. the average of the wavelet power spectrum over time (the dotted line indicates the equivalent global significance level of 95%). The bottom panel shows the variations of the period (thick solid line) of the maximum power peak below the cut-off period (566 s) and its corresponding probability (thin solid line) obtained with the randomization method. There is a standard 3.5% error for the calculated probabilities. The global power spectrum shows a peak of 375 s with a corresponding global probability of 86%.

figuration. In both figures there is clearly a ~ 400 s periodicity present with a high probability for the higher position and a reasonable one for the lower position. A major part of its power lays within the COI and hence maybe subjected to edge-effects, however, its persistence over the whole time series even with a lower power for later times, indicates its physical importance. This period corresponds to the 6-minute oscillations reported for other chromospheric structures such as fibrils, dark grains, mottles (Tziotziou et al. 2004, De Pontieu et al. 2003). Although the aforementioned structures are found in different magnetic field topologies (quiet Sun for mottles and spicules, active regions for fibrils, dark grains and surges), the obtained same period suggests that probably all these structures have the same driving mechanism.

There is also a ~ 120 s periodicity present at Fig. 10 and a ~ 200 s periodicity present at Fig. 9. The latter could probably correspond to the well-known 3-minute chromospheric oscillation.

In Fig. 11 we present the coherence phase derived from the cross-wavelet analysis between the brightness at the mound-top of the inverted “Y” configuration (dashed line in Fig. 8) and brightness at position 8.8''. It is clear that the phase difference is almost constant ($\sim 40^\circ$ in this case) over all periods

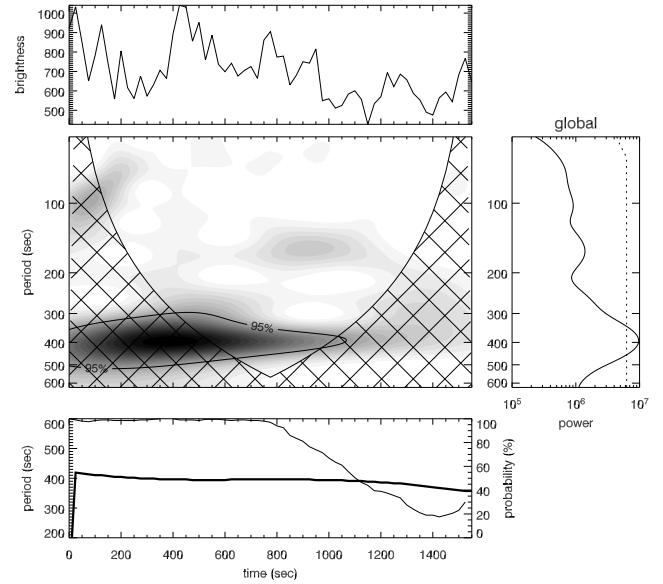


Fig. 10. Wavelet analysis of the brightness (in count) of the surge at position 8.8'' (see Fig. 8). For a description of the presented panels see caption of Fig. 9. The cut-off period is 566 s. The global power spectrum shows a peak of 395 s with a corresponding global probability of 100%.

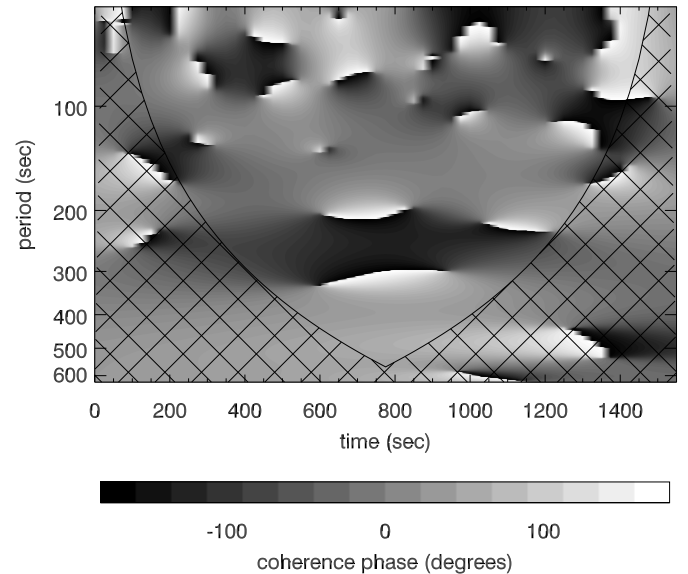


Fig. 11. Coherence phase between brightness at the top of the inverted “Y” configuration (dashed line in Fig. 8) and brightness at position 8.8''. The cut-off period is 566 s.

between 350 and 450 s where the wavelet power of individual series peaks (see Figs. 9 and 10). The same behaviour for phase coherence is found for almost all cross-wavelet spectra along the surge. We will further discuss results about the coherence phase in 4.3.2.

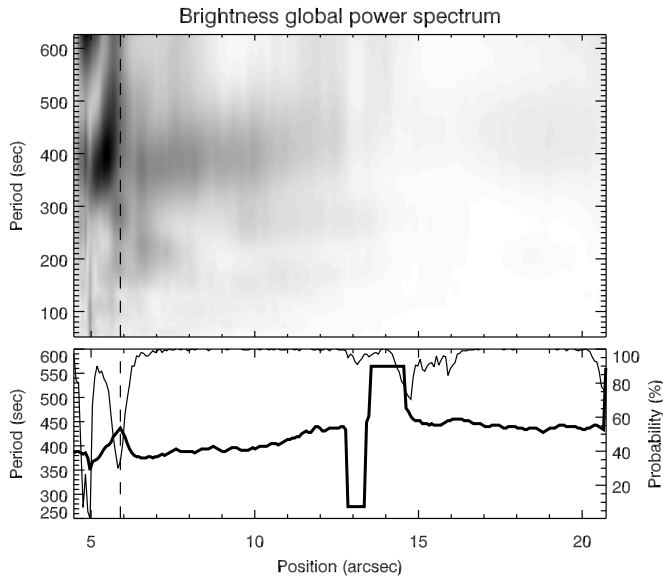


Fig. 12. Wavelet analysis results for the brightness along the main axis of the surge (see Fig. 8). The top panel shows the global power spectrum as a function of period and position along the axis of the surge. The bottom panel shows the variations of the period (thick solid line) of the maximum global power peak below the cut-off period (566 s) and its corresponding probability (thin solid line) obtained with the randomization method. There is a standard 3.5% error for the calculated probabilities. The dark dashed line indicates the mound-top of the inverted “Y” configuration (see Figs. 7 and 8).

4.3.2. Wavelet analysis along the surge

Fig. 12 shows the resulting global power spectra from a wavelet analysis of the brightness along the main axis of the surge (see Fig. 8). The oscillation with a ~ 400 s periodicity is clearly visible for all heights except a short interruption in the range of 12.8 to 14.8”. The power is stronger below the mound-top of the inverted “Y” configuration and then reduces quickly beyond the height of 14” probably due to decreased brightness. There is a trend of a slight increase of period with height with a local maximum also around the mound-top of the inverted “Y” configuration where reconnection is supposed to occur. It is interesting to note that the 3-minute period signature, which is usually associated with the chromosphere, exists only very close to the base of the surge up to a height of ~ 9 arcsec base of which is located very close to “reconnection” Y-shaped base, in accordance with what someone would expect for a structure expanding to the lower corona.????

It is striking that both lower positions which are associated with the reconnection area and the higher positions which are the product of this process (surge) are exhibiting similar period signatures. It seems that the brightness variations within the surge are strongly connected to its driving mechanism. If indeed reconnection is responsible for the creation of the surge then it would push material upwards and downwards from the reconnection site leading to brightness variations along the surge.

The coherence phase from the cross-wavelet analysis between the brightness at the top of the inverted “Y” configura-

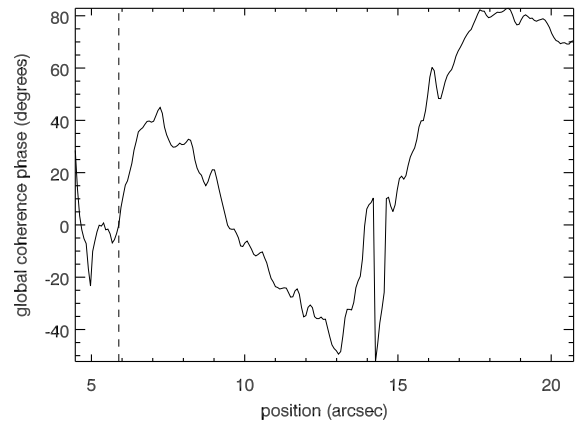


Fig. 13. Global phase coherence (see text) for a period of 400 s as a function of position along the surge. The reference time series is the top of the inverted “Y” configuration (dashed line in Fig. 8). The cut-off period is 566 s.

tion (dashed line in Fig. 8) and the brightness at each position along the main axis of the surge was also calculated (e.g. Fig. 11) and then averaged over time in order to obtain the global phase coherence as a function of period at each position along the surge. In Fig. 13 we present the global phase coherence for a period of 400 s as a function of position along the surge (there are only slight differences of the global phase coherence as a function of position over the period range of 350 to 450 s).

5. Discussion

We present high spatial and temporal resolution observations of the chromospheric limb observed with DOT and the dynamical characteristics of a surge observed both with DOT and TRACE. The observations include the active region AR10486, which later on produced the largest X-flare ever recorded. In DOT images many tiny bright structures around the periphery of sunspot umbrae, but also protruding the limb can be seen with a remarkable clarity. Some of them, despite changes in brightness, are observed to persist for the whole time sequence, while others reappear several times at the same place in periods of a few minutes. The surge is a dynamic structure shrinking and expanding several times at almost the same place. It can be followed for at least 2.5 hours in TRACE images. Since surges are usually suggested to be due to magnetic reconnection this observation indicates that the flux in the interacting magnetic elements is not annihilated all at once. Applying a wavelet analysis in the high-cadence DOT observations we find brightness oscillations with ~ 6 min and ~ 3 min periodicities at some positions within the surge and along the body of the surge. Such oscillations are not uncommon, and have been found in many chromospheric structures, both in quiet (e.g., mottles) and active regions (e.g. fibrils, grains) (De Pontieu et al. 2003, Tziotziou et al. 2004). The exact reason for this periodicity is not easy to be determined without a detailed study of the magnetic footpoints. However, this result points strongly in the di-

rection of a p-mode associated driver, (already suggested for fibrils by De Pontieu et al. 2004).

Apart from the oscillations we also find outward propagating disturbances with different apparent propagation speeds. Such kind of disturbances have already been observed in loops (see e.g De Moortel ...) and in polar plumes (...).

The signal both in oscillations and in propagating disturbances gets weaker as it propagates along the surge and the period of the oscillations increases. At about ... Mm they are not visible any more. Since the length over which oscillations can be detected by the wavelet analysis depends on the amplitude of the oscillation or disturbance and the 99% confidence level the aforementioned result indicates that the amplitude of the signal decreases as it travel along the structure.

An important key is missing from the present observations: observations in different wavelengths together with magnetograms in order to observe features instantaneously in different temperatures, and to determine how the observed pulses are excited. The new capabilities of DOT which now permits the simultaneous 90'' - 70'' FOV in five different wavelength channels together with a sixth camera for Ba II 4554 Dopplergrams and magnetograms are very promising towards this direction.

Acknowledgements. The DOT is operated by Utrecht University at the Spanish Observatorio del Roque de los Muchachos of the Instituto de Astrofísica de Canarias and is presently funded by Utrecht University, the Netherlands Organisation for Scientific Research NWO, the Netherlands Graduate School for Astronomy NOVA, and SOZOU. Wavelet software was provided by C. Torrence and G. Compo and is available at <http://paos.colorado.edu/research/wavelets/>. We thank P. Sütterlin for supplying the data and R.J. Rutten for constructive comments. The DOT efforts and K. Tziotziou's research is funded by the European Commission through the European Solar Magnetism Network (contract HPRN-CT-2002-00313).

References

- Banerjee, D., O'Shea, E., Doyle, J.G., & Goossens, M. 2001, A&A, 371, 1137
- Bloomfield, D.S., McAteer, R.T.J., Lites, B.W., Judge, P.G., Mathioudakis, M., & Keenan, F.P. 2004, ApJ, 617, 623
- Bohlin, J.D., Vogel, J.D., Purcell, N.R., Sheeley N.R. Jr., Tousey, R., & VanHooster M.E. 1975, ApJL, 197, L133
- Canfield, R.C., Reardon, K.P. Leka, K.D., Shibata, K., Yokoyama, T., & Shimojo, M. 1996, ApJ, 464, 1016
- De Pontieu, B., Erdélyi, R., & de Wijn, A.G. 2003, ApJ, 595, 63L
- De Pontieu, B., Erdélyi, R., & James, S.P. 2004, Nature, 430, 536
- Fludra, A. 2001, A&A, 368, 639
- Foukal, P. 1971, Sol. Phys., 19, 59
- Georgakilas, A. A., Koutchmy, S., & Christopoulou, E. B. 2001, A&A, 370, 273
- Handy, B. N., Acton, L. W., Kankelborg, C. C., Wolfson, C. J., Akin, D. J., Bruner, M. E., Carvalho, R., Catura, R. C., Chevalier, R., Duncan, D. W., Edwards, C. G., Feinstein, C. N., Freeland, S. L., Friedlaender, F. M., Hoffmann, C. H., Hurlburt, N. E., Jurcevich, B. K., Katz, N. L., Kelly, G. A., Lemen, J. R., Levay, M., Lindgren, R. W., Mathur, D. P., Meyer, S. B., Morrison, S. J., Morrison, M. D., Nightingale, R. W., Pope, T. P., Rehse, R. A., Schrijver, C. J., Shine, R. A., Shing, L., Strong, K. T., Tarbell, T. D., Title, A. M., Torgerson, D. D., Golub, L., Bookbinder, J. A., Caldwell, D., Cheimets, P. N., Davis, W. N., Deluca, E. E., McMullen, R. A., Warren, H. P., Amato, D., Fisher, R., Maldonado, H., & Parkinson, C. 1999, SoPh, 187, 229
- Kucera, T.A., Andretta, V., Poland, A.I. 1998, Sol. Phys. 183, 107
- Kurokawa, H., & Kawai, G. 1993 in ASP Conf. Ser. 46, The Magnetic and Velocity Fields of Solar Active Regions, eds. H. Zirin, G. Ai, & H. Wang (San Francisco: ASP), 507
- Roy, J.-R. 1973, Sol. Phys. 28, 95
- Roy, J.-R. 1973, Sol. Phys. 32, 139
- Rust, D.M. 1968, IAU Symp. 35, 77
- Rutten, R.J. 1999 in ASP Conf. Ser. 184, Magnetic Fields and Oscillations, eds. B. Schmieder, A. Hofmann & J. Staude, 181
- Rutten, R. J., Hammerschlag, R. H., Bettonvil, F. C. M., Stterlin, P., & de Wijn, A. G. 2004, A&A, 413, 1183
- Schmieder, B., Golub, L., & Antiochos, S.K. 1994, ApJ, 425, 326
- Svestka, Z. 1976, Solar Flares (Dordrecht:Reidel)
- Tandberg-Hanssen, E. 1977, in Illustrated Glossary for Solar and Solar-Terrestrial Physics, ed. A. Bruzek & C.J. Durrant (Dordrecht:Reidel), 106
- Torrence, C., & Compo, G.P. 1998, Bull. Amer. Meteor. Soc., 79, 61
- Tziotziou, K., Tsiropoula, G., & Mein, P. 2004, A&A, 423, 1133
- Yokoyama, T., & Shibata, K. 1996, PASJ, 48, 353
- Yoshimura, K., Kurokawa, H., Shimojo, M., & Shine, R. 2003, PASJ, 55, 313